Journal of Catalysis 282 (2011) 299–309

Contents lists available at ScienceDirect

Journal of Catalysis

journal homepage: www.elsevier.com/locate/jcat

Chemoselective hydrogenation of cinnamaldehyde: A comparison of the immobilization of Ru–phosphine complex on graphite oxide and on graphitic surfaces

A.B. Dongil [a], B. Bachiller-Baeza [a,b,*], A. Guerrero-Ruiz [b,c], I. Rodríguez-Ramos [a,b]

[a] Instituto de Catálisis y Petroleoquímica, CSIC, c/Marie Curie No. 2, Cantoblanco, 28049 Madrid, Spain
[b] UA UNED-ICP (CSIC) Group Des. Appl. Heter. Catal., Madrid, Spain
[c] Dpto. Química Inorgánica y Técnica, Facultad de Ciencias UNED, Senda del Rey 9, 28040 Madrid, Spain

ARTICLE INFO

Article history:
Received 17 May 2011
Revised 5 July 2011
Accepted 5 July 2011
Available online 6 August 2011

Keywords:
Carbon materials
Immobilization
Ru complex
Cinamaldehyde hydrogenation

ABSTRACT

The homogeneous complex $Ru(PPh_3)_3Cl_2$ has been immobilized onto three different carbon materials: graphite, carbon nanofibers, and graphite oxide (GO). All the supports were previously functionalized with (bis(2-aminoethyl)amine). For graphite oxide, a second functionalization strategy using N-[3-(trimethoxysilyl)propyl]-etylenediamine (TPEN) was also followed. XRD, NMR, TG, TPD, DRIFTS, and XPS techniques were applied for the characterization of the functionalized supports and the hybrid catalysts. The hybrid catalysts have been tested in the hydrogenation of cinnamaldehyde and, although less active, they showed selectivities comparables to that for the homogeneous complex. The different behavior observed for the samples after recycling and reusing can be related to the ligand-support interaction type. While activity and selectivity are preserved for the Ru grafted on the covalent-functionalized GO–TPEN, variations in activity and selectivity are observed for the amine-functionalized samples.

1. Introduction

The interest to develop hybrid organic–inorganic catalysts has increased in the last years as it joins the advantages of homogeneous and heterogeneous catalysis, such as the ease of separation from reaction media, and reusability. Several approaches have been investigated for the heterogenization of transition metal complexes on solid supports, being the covalent attachment on micro- and mesoporous inorganic materials the most successful [1,2]. Covalent approach requires the development of grafting and tethering methodologies of which the use of organosilanes agents to react with the surface of different silica-based materials has been the most studied. Additional advantages of the hybrid catalysts derived from site isolation and shape selectivity justify the difficulty on their preparation. In this sense, several publications have appeared where, besides mesoporous materials (MCM-41, SBA-15, etc.), layered compounds, such as clay minerals, are used to improve selectivity since the interlayer space may act as a nanoreactor, where apart from molecular sieving effects the host–guest interactions are enhanced [3,4].

In this context, the high thermal, mechanical, and chemical resistance together with a competitive cost of carbon materials make them ideal candidates to its use as a support to immobilized catalytic homogeneous complexes. However, they have been mainly used as support for metal nanoparticles [5], probably because its high inertness, hydrophobicity, and difficulty to characterize by common spectroscopic techniques have hindered its study. Furthermore, several thermal and chemical processes can be used to tailor the porous structure and the type and concentration of specific oxygen surface groups [6]. A wide variety of oxidizing treatment techniques have been used to functionalize the carbon surface: gaseous (O_2, O_3, CO_2) or liquid (HNO_3, H_2SO_4, H_2O_2) chemicals and electrochemical oxidations, plasma treatment, ion bombardment, etc., the wet oxidation with nitric acid being the most conventional and applied approach. Further modifications of carbon surfaces with other functionalities containing heteroatoms, like N and S, tend to increase their chemical reactivity and give rise to building-blocks or starting materials for subsequent chemical modifications or applications, as the anchoring of metal complexes to the support [7,8].

Among the numerous carbon materials, graphite oxide (GO) can offer further aid to the catalytic selectivity, both owing to the chemical functions at its surface and due to confinement effects. This layered material with a high hydrophilic character due to the epoxy and hydroxyl functionalities placed in the interlayers and carboxylic groups on the edges is obtained after graphite was subjected to strong oxidation conditions. The GO material can develop a rich chemistry, allowing intercalation not only by

* Corresponding author at: Instituto de Catálisis y Petroleoquímica, CSIC, c/Marie Curie No. 2, Cantoblanco, 28049 Madrid, Spain. Fax: +34 915854760.
E-mail address: b.bachiller@icp.csic.es (B. Bachiller-Baeza).

0021-9517/$ - see front matter © 2011 Elsevier Inc. All rights reserved.
doi:10.1016/j.jcat.2011.07.002

ionic exchange but also by covalent bonding through the acidic hydroxyl groups on its layers at the time they expand opening the pore structure. The properties of graphite oxide derivatives depend largely on the synthetic routes including the synthetic method of GO and the reaction conditions [9–12]. On the other hand, it has been reported the reaction of graphite oxide with several alkylchlorosilanes and alkoxysilanes in different solvents concluding that sylilation of graphite via covalent bond (Si–O) was possible when employing high temperature [13,14]. While great attention has been paid to the preparation of intercalated GO composites by incorporation of polar organic molecules, polymers [15], or inorganic materials inside the nanospace of the layers; comparatively few investigations have been made in regard to GO as a host for the intercalation of catalytically active transition and noble metal nanoparticles so far. New hybrid materials consisting on nanoparticles (NPs) anchored onto GO sheets, where the oxygen functional groups act as nucleation centers, have been recently examined [16,17].

An elegant and simple route strategy to immobilize catalytic complexes could be the use of multifunctional molecules, such as organic compounds having two or three amine groups, where one functional group could be used to anchor the molecule to the carbon material and the remaining free groups could react further to anchor the transition metal complex onto carbon surface possible [18,19]. Here, we report the synthesis and catalytic application of hybrid catalysts consisting in a ruthenium(II) complex, $RuCl_2(PPh_3)_3$ anchored onto amine-functionalized carbon materials. In order to study the effect of carbon properties and ligand-support interaction on catalytic performance, we have employed three carbon supports with different morphology: a mesoporous high surface area graphite, a non-porous carbon nanofibers, and a laboratory-prepared graphite oxide, all modified with bis(2-aminoethyl)amine, the two first after a previous oxidation step. For graphite oxide, taking advantage of its rich functionalization (mainly hydroxyl groups), and its laminar character, a covalent approach using an alkoxysilane and the direct intercalation of the complex inside its nanospace was also investigated. All the hybrid catalysts were characterized and tested in the chemoselective hydrogenation of cinnamaldehyde to cinnamyl alcohol.

2. Experimental

2.1. Synthesis and functionalization of carbon materials

Three different carbon materials were studied as starting samples: high surface area graphite, HSAG (S_{BET} = 310 $m^2\ g^{-1}$), from Timcal [20]; commercial carbon nanofiber Pyrograph III, PR24-PS (S_{BET} = 32 $m^2\ g^{-1}$) from Applied Sciences Inc., here denoted as CNF; and laboratory-prepared graphite oxide, GO. Graphite oxide was synthesized from natural graphite powder (99.999% stated purity, −200 mesh, Alfar Aesar) following a modification of the Brodie's method [21]. The graphite was added to a reaction flask containing fuming HNO_3 (200 mL/g of support), which was previously cooled to 0 °C in an iced bath, after that potassium chlorate (8 g) was slowly added. The reaction was left to proceed for 21 h under stirring, and the final solid was filtered, extensively washed with deionized water until neutral pH, and dried under vacuum at 323 K overnight.

Previous to the functionalization with amine, HSAG and CNF were oxidized in concentrated aqueous HNO_3 (1:1 ratio) in order to increase the amount of oxygen-containing groups. While for HSAG, the suspension (10 mL/g of carbonaceous solids) was stirred at RT until total evaporation of the liquid; for the CNF, the suspension was refluxed for 48 h. Both materials were washed in Soxhlet until neutral pH and dried overnight at 383 K. The materials will be denoted as H_{OX} and CNF_{OX}.

Incorporation of the amine (bis(2-aminoethyl)amine) was carried out over H_{OX}, NF_{OX}, and GO samples. H_{OX} and CNF_{OX} supports were suspended in toluene, and an excess of amine with respect to the total amount of oxygen surface groups was added. Then, the mixture was refluxed for 5 h, the solids were filtered and washed in toluene until removal of organics, and finally dried at 383 K overnight. The samples were designated as H_{OX}–T and CNF_{OX}–T. In the case of the GO sample, the method was slightly different. The amine (20 mmol/g GO) was added to a suspension of GO in toluene. After the suspension was stirred at RT for 96 h, the resulting solution was filtered off, and the solid washed with toluene. Finally, the solid was dried in vacuum at 323 K overnight. Sample obtained by this procedure was denoted as GO–T.

Additionally, functionalization of GO with N-[3-(trimethoxysilyl)propyl]-etylenediamine (TPEN) was performed following a similar method to that reported [15]. TPEN (40 mmol per gram of GO) was added to a suspension of GO in toluene. The reaction was maintained at 363 K for 24 h, and after that the sample was filtered, washed in toluene, and finally dried at 323 K under vacuum overnight. This material was denoted as GO–TPEN.

2.2. Anchoring of ruthenium complex

Hybrid catalysts were prepared by adding 0.05 g (1 wt% nominal Ru loading) of commercial complex $Ru(PPh_3)_3Cl_2$ to a suspension of 0.5 g of the support in 20 mL of dichloromethane and maintained at room temperature for 16 h under argon. Finally, the catalysts were washed with dichloromethane and dried under vacuum.

2.3. Characterization techniques

The crystalline phases present in these samples were determined from the X-ray diffraction patterns (XRD). The diffractograms were recorded on a Polycristal ẊPert Pro PANalytical apparatus using Ni-filtered Cu Kα radiation (λ = 0.15406 nm) and a graphite monochromator. For each sample, Bragg's angles between 4° and 90° were scanned at a rate of 0.04°/s.

The amount of oxygen groups present on the surface was determined by thermogravimetric analysis in a CI Electronics microbalance (MK2-MC5). The sample was treated under flowing He for 2 h and then heated at a 10 K min^{-1} rate up to 1023 K. The chemical nature of these functional groups was evaluated by TPD–MS experiments under vacuum in a conventional volumetric apparatus [22] connected to a SRS RGA-200 mass spectrometer. The sample was evacuated for 30 min at room temperature and then ramped to 1023 K at a 10 K min^{-1} rate.

The surface oxidation state was also analyzed by X-ray photoelectron spectroscopy (XPS). The spectra were obtained on a ESCAPROBE P spectrometer from OMICRON equipped with a EA-125 hemispherical multichannel Electronics analyzer. The pressure in the analysis chamber was kept below 10^{-9} Pa. The excitation source was the Mg Kα line ($h\nu$ = 1253.6 eV, 300 W). The binding energy was referenced to the C 1s line at 284.6 eV. The error in determination of electron binding energies and line widths did not exceed 0.2 eV.

High-resolution ^{13}C NMR measurements were performed on a MSL 200 BRUKER spectrometer at 50.3 MHz with magic-angle spinning (MAS). For experiments with proton cross-polarization and magic-angle spinning (CPMAS), the usual contact time was 2 ms. Dipolar dephasing determinations were done to confirm the assignment of the ^{13}C lines deduced from their positions. Measurements were also done with proton decoupling to determine

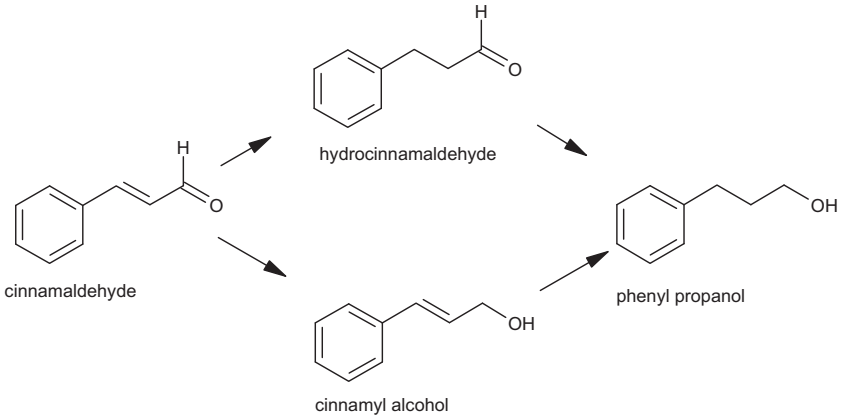

Scheme 1.

the relative amount of the various carbon functions from the intensities of the corresponding lines.

Infrared spectra were collected by using a VARIAN 670 spectrometer equipped with a diffuse reflectance accessory. The diffuse reflectance infrared Fourier transform (DRIFT) spectra were recorded by a MCT detector from 256 scans and with a resolution of 4 cm^{-1}. GO and its derivatives were thoroughly ground and mixed with predried potassium bromide to a final concentration of approximately 1% (w/w).

2.4. Catalytic hydrogenation reaction

The catalytic properties of the hybrid catalysts were tested in the hydrogenation of cinnamaldehyde (Scheme 1). The reaction was carried out in a 300 mL stainless steel Parr reactor at 333 K and 15 bar H_2, and stirring speed 500 r.p.m. Aliquots of the catalyst (200–300 mg), the substrate (0.08 M), 80 mL of isopropanol as solvent and potassium tert-butoxide (70 mg) as base were used in each reaction. Small amounts of samples were taken for analysis by gas chromatography (GC). Analysis of reaction mixture was performed using a Varian 3350 apparatus, equipped with a Carbowax 20 M capillary column and a FID detector. To study the presence of complex on the liquid phase, hot filtration test was performed after every reaction and recycled under the same experimental conditions. The catalyst was also recovered and recycled for the reaction under identical conditions. Catalytic test employing the same amount of the metal complex was also performed homogeneously for comparison purposes.

3. Results and discussion

3.1. Characterization of the functionalized materials

3.1.1. X-ray diffraction

The XRD patterns of H_{OX}, CNF_{OX}, GO and of their derivatives are shown in Fig. 1. Diffraction patterns for graphite and nanofibers series confirm that graphite structure is preserved after oxidation and functionalization as evidenced by the sharp peak at $2\theta = 26°$. On the other hand, the intense and sharp peak of the 0 0 1 reflection centered at $2\theta = 15.8°$ corresponding to an interlayer distance of 0.55 nm (once equilibrated under dry conditions) confirms a high yield in the GO synthesis. XRD patterns of GO derivatives show that intercalation afforded new layered materials with increased interlayer distance compared with GO. Diffraction peaks at $2\theta = 10.2°$ (0.86 nm) and $2\theta = 11.8°$ (0.74) are observed for GO–T and GO–TPEN, respectively. Some areas of these material still preserve the GO structure since a peak at $2\theta = 15.8°$, the same position of the 001 reflection of GO, was observed. The shoulder at 13.2° for GO–T and the small resolved peak at 14° for GO–TPEN could be due to residual solvent molecules intercalated inside the layers. The simultaneous presence of structures with different interlayer spacing that these two samples showed could also be ascribed to different orientations of the intercalated amine molecule, monolayer or bilayer orientation, or bridge or tail conformations as it has been postulated [23]. By assuming a GO layer thickness of 0.07 nm due to the carbon atom, the effective gallery height for accommodating the intercalants in GO–T and GO–TPEN samples is roughly 0.72 and 0.60 nm, respectively. And, taking into account geometric aspects, i.e. size of the amine and TPEN must be >0.75 nm since the length of 3-aminopropyltriethoxysilane is 0.75 nm [24], and the hydrophilic nature of the layers, the intercalants are likely to be in a parallel or titled orientation to yield such *d*-spacing values. Furthermore, a broad hump in the range 18–25° that can arise from GO interstratification is observed more clearly for GO–T. This interstratification is caused by the contraction of unoccupied layers due to the expansion of the filled adjacent layers [25]. The lower angle obtained for GO–T compared to that for GO–TPEN point toward a lower shrinkage of the unoccupied layers.

XRD patterns of the fresh catalysts for the GO series are also displayed in Fig. 1. Intercalated Ru complex on GO showed the broadening of the 002 reflection at 15.9° which can reflect a poorer stacking of layers. Besides, a wide band in the 8.0–11.5° 2θ region appeared. While both Ru–GO–T and Ru–GO–TPEN patterns are similar to those for the corresponding support, retaining the GO structure and with an asymmetric peak at $2\theta = 12°$, probably with two components, the sample prepared on the amine-modified GO showed and intense and wide peak at 24.4° sample. Therefore, the coexistence of different peaks in the patterns indicates that the GO was not delaminated during the preparation process, and the products would have been a random intergrowth of solids with different basal spacings.

3.1.2. NMR spectroscopy

The ^{13}C MAS NMR spectra of GO (Fig. 2) shows two distinguishable signals at chemical shifts 58.6 and 69.8 ppm which have been assigned to 1,2-epoxy and hydroxyl groups, respectively, in qualitative agreement with the model proposed by Lerf et al. [26]. While, conjugated double bonds and un-oxidized sp^2 carbons of the graphene network resonate at 128.4 ppm. The signals at 229 and 29 ppm could be assigned to spinning side bands of the C=C bonds in the condensed aromatic structure. On the other hand, carboxylic groups are probably below the detection limit of solid NMR. Sample GO–T also presented the peaks at 59.2, 69.1, and 124.5 ppm, and an additional peak at 162 ppm. The reduction in

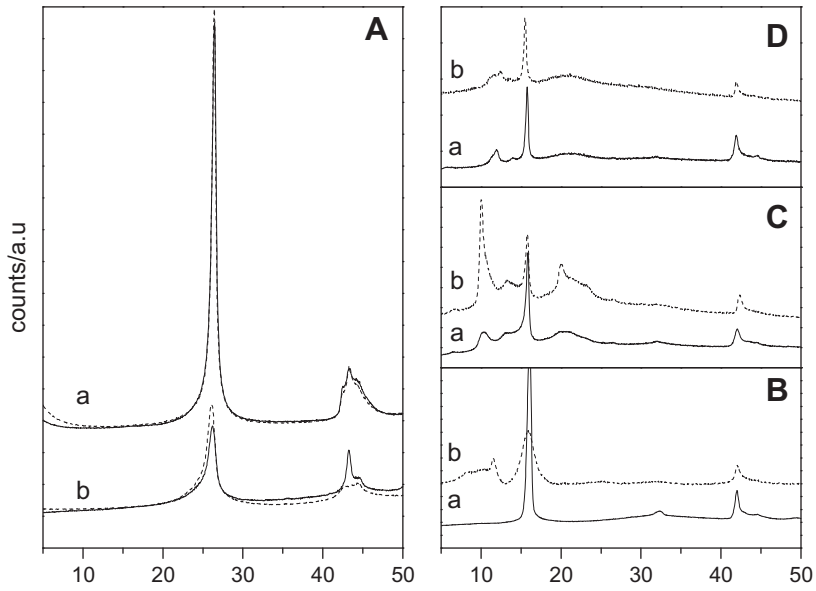

Fig. 1. XRD patterns for (A) HSAG (a) and CNF (b) series, (—) original and (- - -) oxidized samples, and (B), (C), and (D) graphite oxide series (bottom GO, middle GO–T, and top GO–TPEN), (—) support and (- - -) catalyst.

the intensity ratio of the peaks assigned to C–OH and C–O–C carbons added to its lower resolution indicates a loss in the amount of oxygen groups. The prominent feature at 124.5 ppm is broadened by chemical shift distribution and probably corresponds to variations of carbon atom environments due to the intercalation of the amine, which may be interacting with remaining oxygen groups. The appearance of the signal at 162 ppm added to the loss of intensity of the peak at 59.2 ppm could be indicative of glyoxime groups formed by nucleophilic attack of the amine to the epoxy groups [26]. Furthermore, the long tail at low resonance observed for the band at 58.6 could suggest the contribution of the amine molecule to the spectra. ^{13}C NMR of GO–TPEN sample also showed a decrease in intensity for the –OH and C–O–C signals which are less resolved and the maxima are at 70.7 and 58.2 ppm, respectively. The peak at 58.2 ppm also presents a longer tail that could be due to the characteristic spectral features of the intercalat that lie in this region [27].

^{29}Si NMR of this immobilized ligand (Fig. 3) shows us two peaks at −62 and −70 ppm that indicates different forms of silicon species. Following similar considerations as for silica materials they could be assigned to T^2 and T^3 silicon environments, respectively [28], corresponding to the alkoxysilane condensing with two and

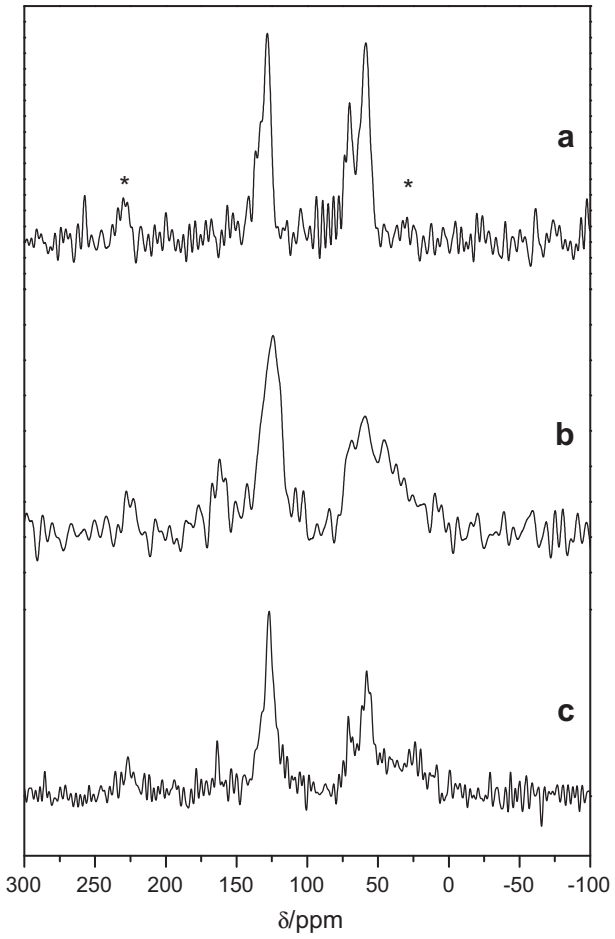

Fig. 2. ^{13}C MAS NMR spectra for samples: (a) GO, (b) GO–T, and (c) GO–TPEN. (*) spinning side bands.

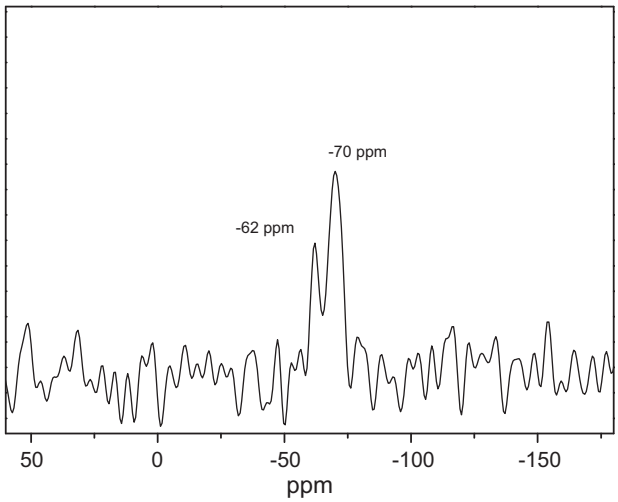

Fig. 3. ^{29}Si MAS NMR spectra for GO–TPEN sample.

three –OH groups structures as shown in Scheme 2. Therefore, it is confirmed the covalent attachment of the alkoxyde to the carbon surface and, taking into account the relative ratio between both species, mainly by means of three OH groups. Lateral and vertical polymerization creating polysiloxanes through the formation of intermolecular bonds, as it has been proposed on SiO_2 surfaces [29], could be disregarded taking into account the limited amount of residual water on the support and the final basal spacing obtained.

3.1.3. Thermal analysis

The oxidized and the modified samples were characterized by thermal analyses, and Fig. 4 displays the thermogravimetric (TG) curves. The TG profiles for H_{OX}, H_{OX}–T, CNF_{OX}, and CNF_{OX}–T are displayed in Fig. 4 A. Both oxidized samples show constant rates of weight loss during the whole profile. However, the total weight loss for sample CNF_{OX}, 9%, was higher than for H_{OX}, 7%, implying a higher amount of surface oxygen groups. Both amine-modified samples showed similar behavior with profiles having a drop in the 473–673 K range, more marked in the case of CNF_{OX}–T, and with total weight loss higher than that obtained for the oxidized samples, confirming the presence of the amine on the graphite and carbon nanofiber surfaces. The weight loss at 473 K has to be assigned to the desorption–decomposition of the surface complexes formed after amine incorporation. Moreover, the higher amount of amine retained in CNF_{OX}–T was consistent with its higher density of oxygen-containing groups.

For GO sample (Fig 4B), after a small initial weight decrease due to the adsorbed water, the sample showed a strong decrease at 535 K. This weight loss corresponds to the release of different gases during the reductive exfoliation of GO that takes place at this temperature. The exfoliation process is associated with the thermal expansion of the evolved gases trapped between the graphene sheets. These evolved gases are H_2O, CO, and CO_2, as it is suggested by the TPD profile (see below), which are consequence of the decomposition of the oxygen-containing functionalities present on the GO sample, mainly ether and OH groups. The weight loss of this stage is nearly 30%. For higher temperatures, the weight loss followed a slower rate, and a total mass loss of about 40% is eventually reached. The profile for GO–T shows that the temperature of the main weight loss, which is representative of the temperature of exfoliation, was shifted to lower values. The smooth decrease from 420 K to 540 K seems to contain two drops at 470 and 520 K. While the latter drop is consistent with the temperature of exfoliation of unoccupied galleries just as the XRD patterns suggested, the first would be due to the evolution of gases coming from the oxygen groups and amine decomposition in the amine-intercalated areas. This observation is consistent not only with the increase in the interlayer distance after intercalation of the amine molecules, but also with the reducing power of the intercalated molecule. It has been reported that the higher the reducing power of the intercalated molecule, the lower the exfoliation temperature [30]. Moreover, the elimination of some of the oxygen-containing groups from the GO occurring after reaction with the amine can be inferred since the total weight loss has been unaltered, and in this

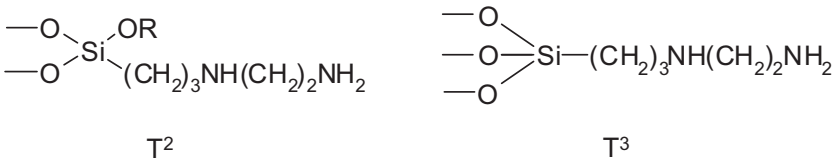

Scheme 2.

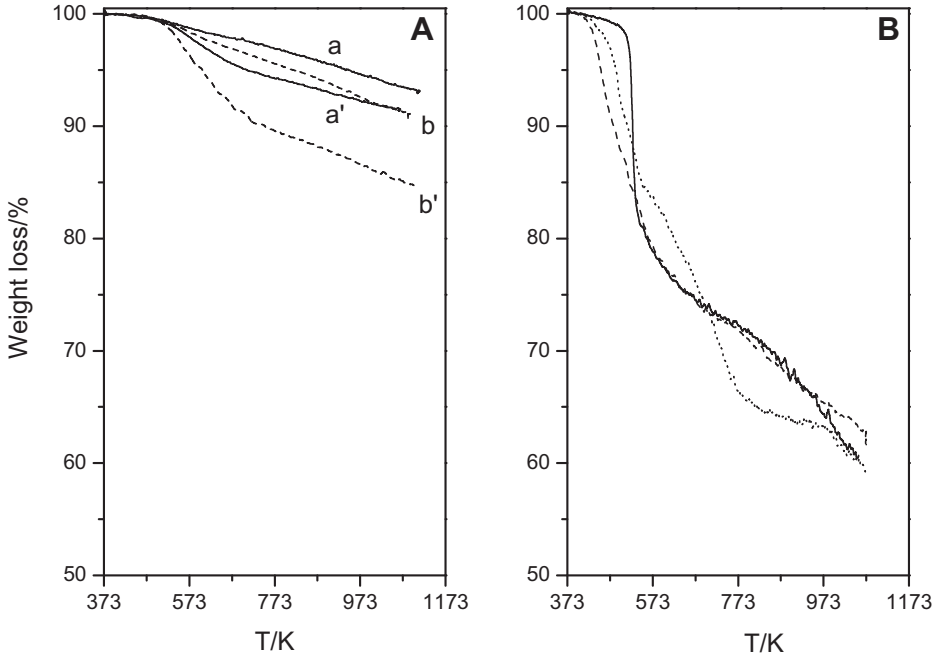

Fig. 4. Thermograms in inert for (A) H_{OX} and H_{OX}–T, solid lines (a) and (a′), respectively, and CNF_{OX} and CNF_{OX}–T dashed lines (b) and (b′), respectively, and (B) GO (—), GO–T (- - -) and GO–TPEN (···).

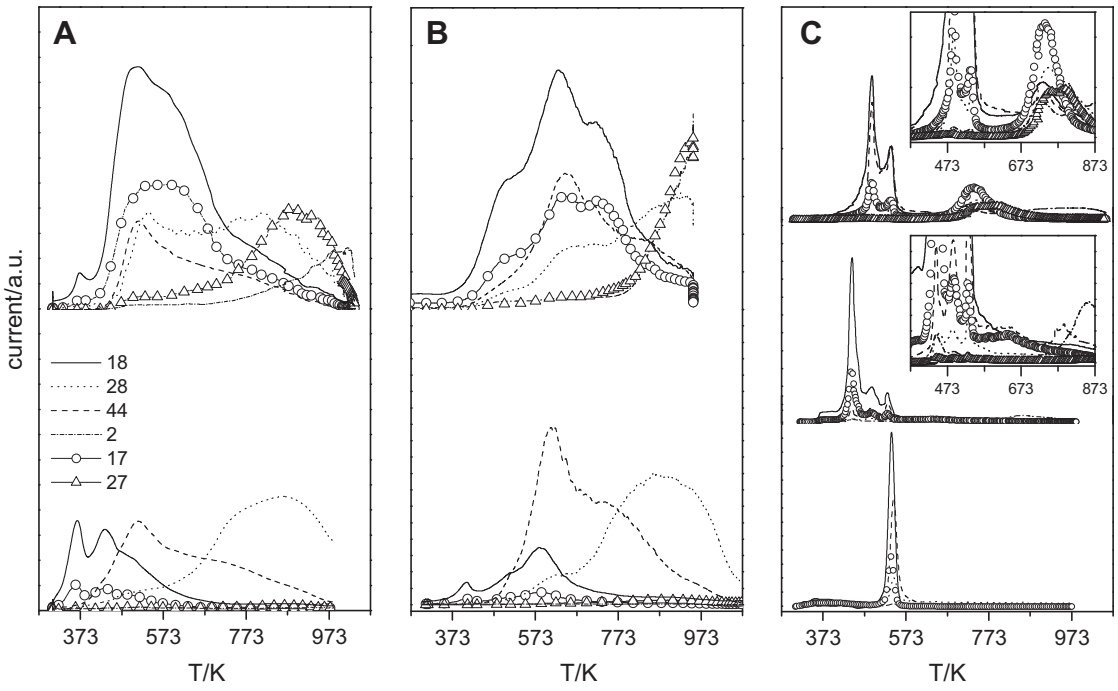

Fig. 5. TPD for (A) HSAG and (B) CNF series (bottom oxidized samples and top amine-modified samples), and (C) graphite oxide series (bottom GO, middle GO–T, and top GO–TPEN).

case, it must be assigned to two processes, the decomposition of the amine and evolution of oxygen groups. Three different small drops can be observed for GO–TPEN: at 490 K, 529 K, and in the 560–773 K range. While the two first can be assigned to the exfoliation and evolution of oxygen groups of layers with intercalated TPEN and original GO sheets, the later is assigned to the decomposition of the anchored TPEN on the delaminated layers as the TPD suggests, see below.

The analysis of the gases evolved during the temperature-programmed desorption (TPD) experiments was also studied. The TPD profiles for samples H_{OX}, H_{OX}–T, CNF_{OX}, and CNF_{OX}–T, GO, GO–T, and GO–TPEN are displayed in Fig. 5. For the amine-modified samples, the fragmentation pattern in the mass quadrupole of the studied amine was considered and therefore, some other masses were monitored during the TPD to study their contribution to the general spectra. To asses for evolution of molecularly adsorbed amine, we have selected signal m/z 73, which contributes to the triamine fragmentation pattern with a 70.4%, because its major fragment $m/z = 44$ can be masked by the CO_2 contribution. The lack of m/z 73 during the TPD suggests that molecular evolution of physically adsorbed amine is not taking place and can be taken as a proof of other kind of interactions responsible of the attachment of the amines to the surface of the materials. Samples H_{OX}–T and CNF_{OX}–T have a similar thermal behavior. Comparing the profiles for the amine-modified samples with those of the oxidized materials, an intense and wide signal for m/z 18 is obtained. Although this mass is generally assigned to water desorption, the temperature is quite higher than that expected for physisorbed water. Other important features are the increase in $m/z = 28$ intensity at temperatures lower than 673 K and the appearance of $m/z = 2$ and $m/z = 27$ at temperatures higher than 773 K. All these facts seem to point toward the contribution of the amine thermal decomposition during the TPD experiment. Furthermore, the slight decrease in the intensity of signal $m/z = 44$ at temperatures lower than 673 K could be taken as an indication of the carboxyl groups are involved in the anchoring of the amine molecule.

The profile for the GO sample, Fig. 5C, shows intense signals for m/z: 18, 44, and 28, which can be assigned to H_2O, CO_2, and CO, respectively, coming for the decomposition of the oxygen functional groups. The temperature of the decomposition peak corresponds to the value obtained in the TG profile, i.e., 535 K. The general spectra change for the intercalated samples. While for the amine-modified sample, GO–T, the TPD showed three peaks in the range 440–540 K, at 440, 490, and 530 K, for the TPEN sample it displays two main peaks in that range, at 490 and 540 K, and an additional peak at higher temperatures, centered at 740 K. The masses that mainly contribute to the profile were 18, 17, and 44 and 28 as it was also seen for the graphite and carbon nanofibers samples. The temperature of the latter peak for both samples, i.e., 530–540 K, coincides with the temperature of GO exfoliation. Thus, this peak must be attributed to decomposition of functional groups in the residual not intercalated GO structures, which were also detected by XRD. A tentative assignment for the other peaks, peak at c.a. 440–500 K and the additional peak at 740 K for TPEN-modified sample, can be made. It is reasonable to assign the peak at 440 K for GO–T and at 490 K for GO–TPEN to the exfoliation and decomposition of oxygen groups of the layers, OH and epoxy groups, where the molecules are intercalated. While for GO–T sample, the simultaneous decomposition of the amine would contribute to this peak; for GO–TPEN sample, TPEN would still be covalently anchored to the graphite oxide layers after exfoliation. Therefore, the peak at 740 K could be attributed to different fragments evolved from the anchored-TPEN decomposition. The additional peak observed at 490 K for the triamine-modified sample could be due to the exfoliation of layers occupied with residual toluene molecules. Contrary to what it was seen for the graphite and nanofiber series, $m/z = 27$ is absent for GO–T. So the coordinated amine molecules undergo different chemical transformations leading to the desorption of other products.

Summarizing, the different thermal stability as well as the different mechanism of decomposition upon heating of the amine species for H_{OX} and CNF_{OX}, and GO reveal that amine molecules

are coordinated to different sites. The reaction pathways for amine degradation can be complex and can include: Hofmann elimination to form alkylamine and unsaturated hydrocarbon, dehydrogenation to form imines or nitriles and disproportionation, depending on the type of interaction with the support and with the surface sites [31,32]. These latter are in this case the oxygen-containing groups present on the original materials. These species could be subsequently decomposed to other products that could be incorporated on the carbon matrix [31] or readsorbed on other sites leading to different secondary products after decomposition. For graphite and nanofibers, the amine seems to form a carboxylate salt with the carboxylic acids [33]. The carboxylate can be in part thermally condensed to amide during the TPD run and finally decomposed leading to HCN at high temperature [34]. Moreover, Schiff condensation between the amine groups and the surface carbonyl groups [7] cannot be disregarded considering the decrease in the intensity of m/z 28 of the corresponding TPD profiles. Although graphite oxide also presented carboxylic and carbonyl groups on the edges of the layers, they are in low amounts compared to the majority groups, i.e., the less thermally stable hydroxyl and epoxy groups. Then, for these materials, the amine seems to be in equilibrium between hydrogen bonded and protonated species formed with the acidic C–OH groups [35]. These species decompose in ammonia and olefins following a reaction similar to Hofmann elimination as has been described for other acid materials [36].

3.1.4. DRIFT spectroscopy

The chemical modification obtained for the samples was studied by IR measurements. FTIR spectra for HSAG and CNF series are shown in Fig. 6. Oxidized samples showed bands at 3400 cm^{-1} (O–H), 1720 cm^{-1} (C=O), 1380 cm^{-1} (C–OH), and 1575 cm^{-1} (Csp^2–Csp^2). Very small differences were found for the spectra of H_{OX}–T and CNF_{OX}–T comparing with those of the corresponding oxidized samples. While the band at 1720 cm^{-1} related to C=O of COOH groups is reduced, a new shoulder or band at 1645 cm^{-1} derived of amino groups is observed particularly for H_{OX}–T. These two features would confirm the incorporation of the amine to the original materials. However, the assignation of the species formed is not conclusive since no other bands are distinguishable.

DRIFT spectrum of GO presents characteristic features in agreement with previous works [37,38,10]. The intense bands at 3627, 3490, 1578, and 1383 cm^{-1} are attributed to stretching and bending vibrations of the acidic C–OH groups, while band at 1713 cm^{-1} is associated with stretching of the C=O bond of carbonyl and/or carboxyl groups situated at the edges of the lamellae, and the intense band at 1063 cm^{-1} due to deformation of the C–O bond of epoxy functionalities. Contributions of skeletal vibrations of un-oxidized graphitic domains to the peak at 1578 cm^{-1} cannot be disregarded [38]. The general spectra changed after modification with amine and TPEN. For GO–T sample, the bands at 3627, 3490, 1578, and 1383 cm^{-1} derived from the hydroxyl groups are reduced severely and the band at 1713 cm^{-1} due to carbonyl and/or carboxyl groups disappeared. While the peaks at 1280 and 1058 cm^{-1} still indicated the presence of the C–O–C groups. In addition, other features related to the presence of the amine can be detected. The band with the maximum at 3490 cm^{-1} is broader and has been shifted to lower wavenumber, which can be an indication of NH_2 moieties. Peaks at 1667, 1560, 1450, and 1193 cm^{-1} appeared. While the peaks at 1667 and 1560 cm^{-1} can be assigned to asymmetric and symmetric deformation bands of hydrogen-bonded NH_2 of the amine molecule interacting with the acidic hydroxyl groups [35], the bands at 1450 and 1193 cm^{-1} could be assigned to δCH_2 [23] and ρNH_2, respectively. The peaks assigned to asymmetric and symmetric stretching vibration of CH_2 groups from the amine molecule, 2940 and 2865 cm^{-1}, would be overlapped by the broad O–H and N–H band. However, the appearance of the new peaks added to the fact that the C=O stretching vibration is absent or shifted to lower wavenumber could be also attributed to the formation of an amide bond between the amine and the carboxylic groups on the edges. And therefore, the bands at 1667 cm^{-1} and at 1560 cm^{-1} would have some contribution of the amide carbonyl-stretching mode and of the coupling of the C–N stretching vibration with the CHN deformation vibration, respectively [39]. The band at 1058 cm^{-1} peak that is

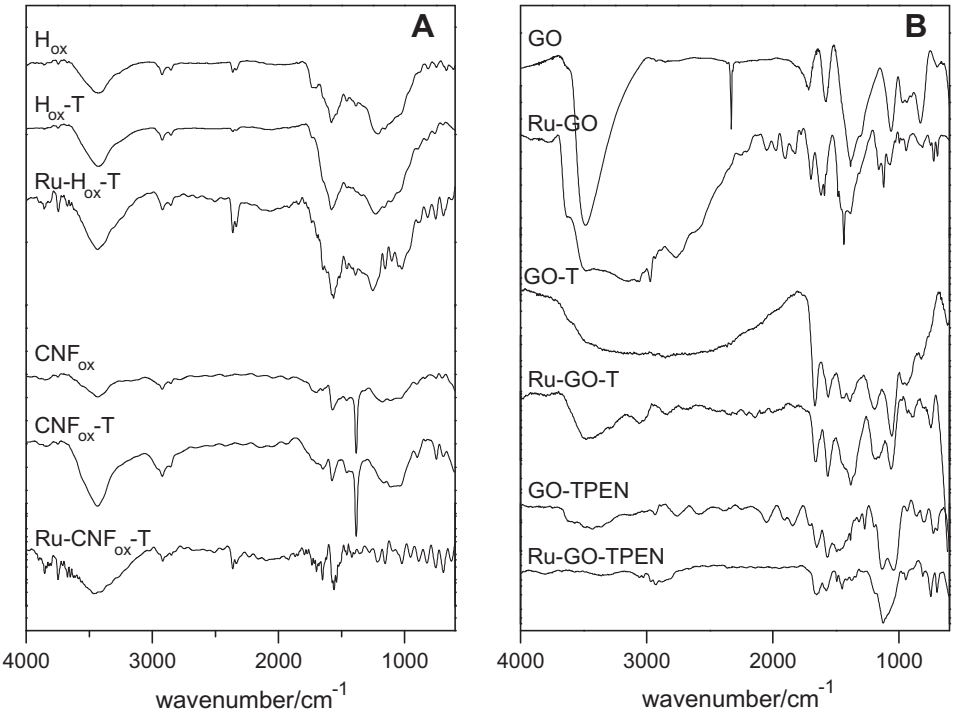

Fig. 6. FTIR and DRIFT spectra for the supports and hybrid catalysts.

associated to the epoxy groups was almost unchanged, which seems to exclude the nucleophilic attack of the amine to the epoxy groups. Besides, for GO–TPEN bands due to –OH disappear completely and apart from the same bands observed on GO–T at 1656, 1565, 1450, and 1196 cm^{-1} ascribable to the amine groups, new bands at 1496, 1319, 1273, and 1122 cm^{-1} are observed. The assignment of the new bands at 1496, 1319, and 1273 cm^{-1} is uncertain but one possibility is that they are due to some intramolecular interaction, hydrogen bond of the amine groups with the aminosilane's silanol groups, or due to the formation of protonated amine groups. The band at 1122 cm^{-1} is assigned to Si–O bonding which would confirm condensation through hydroxyl groups. In addition, the shift to lower wavenumber, 1038 cm^{-1}, of the band attributed to C–O possibly indicates some additional contribution of Si–O bonds from remaining CH_3O–Si.

DRIFTs spectra of the catalysts (Fig. 6) clearly confirm the presence of ruthenium complex on the surface. Bands at 3030–3070 cm^{-1} (ν C–H in Ph), 1493, 1440 (ν C–C), 1086 cm^{-1} (P–Ph), 750–700 cm^{-1} (δ C–H in Ph) characteristic of the $[RuCl_2(PPh_3)_3]$ complex are present in every catalyst [40,41].

3.1.5. X-ray photoelectron spectroscopy

Analysis of the XPS spectra for the modified samples H_{OX}–T, CNF_{OX}–T and GO–T and GO–TPEN clearly evidenced the presence of amine on the surface, since a new peak in the 400 eV region, corresponding to N 1s transition, is observed. The relative amounts of the different species, C, O, and N, were calculated from the corresponding peak areas divided by the sensitivity factors (1.00 for C, 2.85 for O and 1.77 for N) and are shown in Table 1. The O/C ratios obtained for the series showed a small decrease in the oxygen content after the functionalization with amines at expenses of an increase in the N/C ratio, which agrees with the incorporation of the amine. This N 1s region (Fig. 7) showed a broad peak for all the modified samples indicating that several N species contributed to the signal. The type of species depends on the material as the TPD showed. Therefore, two components assigned to free $–NH_2$ groups (N1 at 399.5 eV) and to the ammonium salt (N2 at 400.5 eV) formed via the acid–base reaction between the amine and the carboxylic groups located on the borders of the graphene sheet can be postulated for H_{OX}–T and CNF_{OX}–T. While for H_{OX}–T, the N1/N2 ratio agrees quite well with the expected value taken into account the number of $–NH_2$ groups of the molecule, the lower N1/N2 ratio for CNF_{OX}–T could be due to interactions between adjacent groups favored by the proximity of amine molecules to each other or to the formation of cycled species due to the higher density of COOH groups comparing with the graphite derived sample (see below the relative peak areas for O 1s region).

On the other hand, two contributions assigned to neutral amine (N1′ at 399.7) and protonated amine (N2′ at 400.9) can be suggested for GO although in this case, the latter would be due to the interaction with the –OH groups. The open layered structure of the GO materials can allow intercalation of the amine interacting with two adjacent layers at the same time which would explain the N1′/N2′ ratio lower than 2. The existence of hydrogen-bonded NH_2 as it has been proposed [35] cannot be disregarded taking into account the slightly higher BE for N1′ comparing with those of the graphitic samples. More interesting is the spectrum for GO–TPEN where the peak showed a tailing at high BE. This seems to indicate that a third type of species contributes to the spectra, which probably results from the intramolecular interaction of the amine group and silanol groups of the alkoxide.

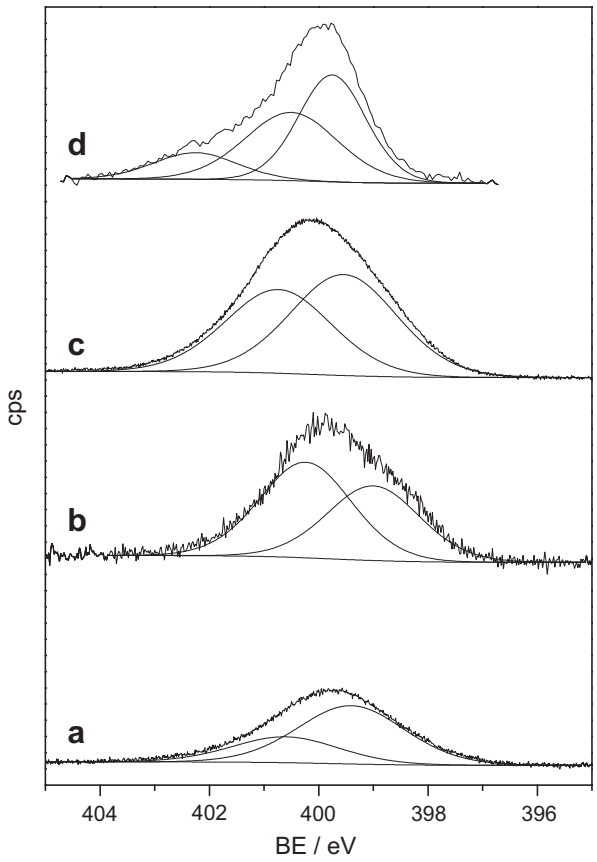

Fig. 7. N 1s spectra for H_{OX}–T (a), CNF_{OX}–T (b), GO–T (c), and GO–TPEN (d).

Some other qualitative features that support these facts can be envisaged after analysis of the C 1s (Fig. 8A) and O1s (Fig. 8B) peaks. The C 1s spectra for HSAG and CNF series showed a broadening of the main peak in the 286–288 eV region, where C 1s core levels of the amine and amide bonds lie. In addition, a decrease in intensity at 289.3 eV, which is in agreement with carboxylic–amine interaction, was observed. Quantitative determinations could not be unambiguously made due to the overlapping of the C–N species with those for C–O and C=O groups. The position of the maximum for the C 1s spectra of GO sample indicated a major contribution of the component assigned to defects. This was expected considering that the structure of the graphite oxide is mainly formed by sheets of graphene that have lost their aromatic character due to the creation of epoxy and hydroxyl groups. Moreover, this is corroborated by the absence of the $\pi \rightarrow \pi^*$ peak characteristic of large polyaromatic structures. The asymmetry of the peak in this case is a consequence of the high proportion of oxygen groups as the O/C ratio has indicated. After the incorporation of amine or alkoxide on GO, the maximum of the C 1s spectra is shifted to higher BE, which is due to the presence of C–N structures, and the $\pi \rightarrow \pi^*$ peak is insinuated indicating the partial recovery of the aromatic character.

Table 1
XPS data of the supports.

Sample	S_{BET} ($m^2\ g^{-1}$)	O/C	N/C	N1/N2	Relative peak area (%)		
					Peak A C=O	Peak B CO	Peak C COOH
H_{OX}	167	0.05	–	–	35	39	26
H_{OX}–T	112	0.04	0.04	2.1	51	36	14
CNF_{OX}	42	0.19	–	–	30	30	40
CNF_{OX}–T	37	0.10	0.22	0.8	75	19	6
GO		0.22	–	–	17	55	28
GO–T		0.15	0.27	1.1	66	28	6
GO–TPEN		0.25	0.20	1.7	10	81	8

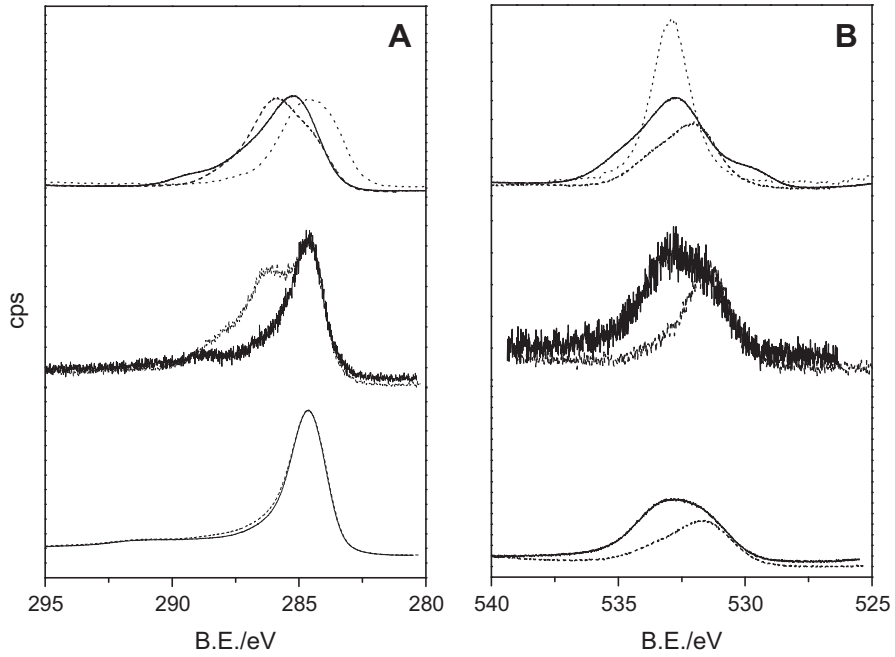

Fig. 8. (A) C 1s and (B) O 1s spectra for HSAG (bottom), CNF (middle) and GO (top) series. (—) Unmodified, (- - -) amine-modified and (···) TPEN-modified sample.

As far as the O1s region is concerned, the shift of the maximum to lower BE upon incorporation of the amine on the graphite and carbon nanofiber series indicated that modifications in the relative proportion of the different components occurred. The O 1s peak can be deconvoluted in three components: carbonyl oxygen (peak A, 531.4); oxygen atoms in C–O bonds like hydroxyl and ether groups (peak B, 532.6); oxygen atoms in acidic carboxyl groups (peak C, 534.6). Table 1 shows the relative area of the different peaks. There is a marked increase in the ratio of Peak A at the expense of a reduction in the Peaks B and C, being the latter assigned to the carboxylic acids. This would confirm again the participation of the –COOH groups in the anchorage of the amine for H_{OX}–T and CNF_{OX}–T. As far as the GO samples is concerned, the data for the amine-modified sample also suggest a decrease in the proportion of carboxyl groups that goes along with an increase in the C=O type groups. However, for OG–TPEN sample, the increase in the proportion of C–O bonds seems to corroborate the attachment of the alkoxide.

XPS analyses showed further evidence for the successful anchoring of the $RuCl_2(PPh_3)_3$ complex. Table 2 includes Ru 3p3/2 (Ru 3d5/2 is overlapped by C1s), N 1s, and P 2p core level binding energies (BE). The Ru 3p3/2 BE values in the range 462.9–463.3 eV, and the P 2p BE values are consistent with those obtained from Ru^{II}–phosphine complexes [42]. This would confirm the presence and integrity of the $RuCl_2(PPh_3)_3$ complex when anchored into the supports. Besides, maximum for N1s peak (not shown) is slightly shifted to higher B.E after complex immobilization which can be related to changes in the proportion of the amine species due to coordination of N atoms with the Ru^{II} nuclei [41].

3.2. Hydrogenation reactions

The hybrid catalysts were tested in the chemoselective hydrogenation of cinnamaldehyde, and Table 3 includes the results of activity and selectivity to the unsaturated alcohol, cinnamyl alcohol. For comparison, the homogeneous complex $Ru(PPh_3)_3Cl_2$ was tested under the same reaction conditions. The activity values were calculated as mol of cinnamaldehyde converted per mol of Ru and reaction time at 50% conversion, considering the nominal Ru content of 1%. The hybrid catalysts proved to be active and very selective to the unsaturated alcohol. The activity values followed the trend: homogeneous > Ru–H_{OX}–T > Ru–GO > Ru–GO–T > Ru–CNF_{OX}–T > Ru–GO–TPEN. All the catalysts presented are less active than the homogeneous complex, probably due to diffusion limita-

Table 2
XPS data of the hybrid catalysts.

Catalyst	Ru $3p_{3/2}$ B.E. (eV)	P 2p B.E. (eV)	N 1s B.E. (eV)	Ru/C	N/C	O/C
Ru–H_{OX}–T	463.2	132.5	400.3	0.001	0.03	0.04
Recycled	463.1	132.3	400.3	0.001	0.03	0.03
Ru–CNF_{OX}–T	462.9	132.7	399.9	0.004	0.17	0.11
Recycled	462.8	132.6	399.8	0.003	0.15	0.14
Ru–GO						
Recycled	463.3	133.2	–	0.001	–	0.06
Ru–GO–T	n.d.	n.d.	n.d	n.d.	n.d.	n.d.
Recycled	462.3	131.4	399.9	0.002	0.08	0.08
Ru–GO–TPEN	463.2	132.8	400.2	0.003	0.09	0.23
Recycled	463.1	132.6	399.7	0.003	0.07	0.13

Table 3
Catalytic results for the fresh and recycled catalysts.

Catalyst	Cycle	Half reaction time (h)	Selectivity (%)	Activity[a]
Homogeneous	1	3	70	36.0
2Ru–HSAG[b]			38	12.0
Ru–H_{OX}–T	1	3	55	31.5
	2	5	76	21.4
Ru–CNF_{OX}–T	1	21	87	5.1
	2	26	88	4.1
Ru–GO	1	8	71	12.7
	2	12	72	8.5
Ru–GO–T	1	15	80	7.1
	2	15	69	7.1
Ru–GO–TPEN	1	25	87	4.3
	2	25	88	4.3

[a] Calculated as [mol converted/(mol Ru nominal * h)] at 50% conversion.
[b] Results for Ru nanoparticles supported on HSAG taken from [43]. The activity was recalculated at 50% of conversion.

tions as it is usually observed in heterogenized complexes. The higher activity obtained for Ru–H_{OX}–T, which showed lower Ru content by XPS, could be due to the higher accessibility of the reactant to the active site. For the GO series, it seems that the presence of ligand, triamine, or TPEN on the interlayer surfaces hinders the diffusion of reactant and/or products in the interlamellar space, since Ru–GO prepared via direct intercalation showed the highest activity among the GO supported samples.

As far as the selectivity is concerned, cinnamylalcohol was the main product of the reaction for all the catalysts. The selectivity values for the hybrid catalysts in the range 80–87% were higher than for Ru nanoparticles supported on graphite (38%) [43], higher than for the homogeneous catalyst except for Ru–H_{OX}–T (55%) and Ru–GO (70%), and similar to Ru–SiO_2–TPEN and other silica systems found in the literature [41]. Moreover, while selectivity to cinnamylalcohol was constant with reaction time for Ru–CNF_{OX}–T, Ru–GO, Ru–GO–T, and Ru–GO–TPEN, conversion of cinnamylalcohol to the saturated alcohol was observed for Ru–H_{OX}–T at CAL conversions higher than 60%. The higher selectivity obtained for the hybrid catalysts is related to the presence of $–NH_2$ or –NH– groups of the triamine ligand. In fact, catalyst Ru–GO where the amine is absent showed the lowest selectivity among the heterogenized samples (excluding Ru–H_{OX}–T) and similar to that for the homogeneous system and seems to reflect that not additional steric effects due to the confinement of the complex in the interlayer of the GO have to be considered. These amine groups activate the reactant C=O bond by forming a hydrogen bond (–NH···O) and give the adequate spatial arrangement for the hydrogen transfer [44]. This reaction mechanism is the difunctional metal–ligand proposed by Noyori and Ohkuma [45] and adapted for cinnamaldehyde in heterogenized systems by Ghosh and Kumar [41] in which the reactant interacts with the ligand and not directly with the metal center. Therefore, taking into account that the amine interaction is similar for both H_{OX}–T and CNF_{OX}–T supports, the lower selectivity obtained for Ru–H_{OX}–T compared to that for Ru–CNF_{OX}–T can be due to the direct anchoring of the complex to functionalities different than the amine, i.e., oxygen groups. While, very small differences are observed for Ru–OG–T and Ru–OG–TPEN despite the different ligand-support interaction.

In order to prove that the reaction was catalyzed heterogeneously and to exclude the possibility of homogeneous catalysis, the reaction mixture was separated from the catalyst before complete conversion occurred (hot filtration test), more reactant added to the filtered and tested under reaction conditions. The absence of reaction of the filtered sample proved that no homogeneous catalysis took place except for Ru–GO sample which gave a conversion of 20% after 30 h and remains at this value after that time.

In addition, the stability of the materials was studied by recycling the catalysts in a second run. While Ru–H_{OX}–T, Ru–CNF_{OX}–T, and Ru–GO showed a reduction in activity of 20–30%, Ru–GO–T, and Ru–GO–TPEN showed similar activity values. As far as the selectivity to cinnamylalcohol is concerned, Ru–CNF_{OX}–T, Ru–GO, and Ru–GO–TPEN showed the same values obtained in the first run, the values for Ru–GO–T were slightly reduced and for Ru–H_{OX}–T selectivity increased up to 76%. The XPS data of the recycled catalysts (Table 3) confirm the presence of the metal complex since the Ru/C and atomic ratios did not vary and neither the BE values for Ru or P. The increase in the selectivity to cinnamylalcohol observed for the recycled Ru–H_{OX}–T could be related to the changes in the metal coordination sphere after incorporation of solvent molecules or ligands elimination. However, since the BE of the Ru 3p3/2 transition does not change significantly after recycling, it seems more probable that the metal complex anchored on the oxygen surface groups and not selective is removed during the first run. This would explain both the reduction in activity and the increase in selectivity.

For the GO series, the lower activity for Ru–GO is probably due to the leaching of the complex due to the low interaction with the support. The partial loss of amine during the reaction for Ru–GO–T due to its higher mobility in the interlamellar space could explain the lower selectivity values for the recycled sample. This fact seems to be corroborated by the lower N/C ratio observed for the recycled catalyst comparing with that for the original support. Furthermore, the heterogeneous distribution of the amine in the interlayers as the XRD reflected can imply areas of the sample where the metal complex is intercalated in non-functionalized surfaces, giving selectivities similar to that of the homogeneous complex. On the other hand, Ru–GO–TPEN being the less active sample is the most stable catalyst in terms of activity and selectivity. Furthermore, comparing the DRIFT spectra for the recycled catalysts with those for the fresh catalysts, it can be observed that while the spectra for Ru–GO and Ru–GO–T have changed considerably, only Ru–GO–TPEN preserved all the signals that assesses the complex attachment, i.e., 3058, 3028, 1450, 750, and 699 cm^{-1} and agrees with its stability.

4. Conclusions

Inmobilization of $Ru(PPh_3)_3Cl_2$ onto carbon materials have been achieved by heterogenization onto amine-modified graphite oxide, carbon nanofibers, and graphite, being the two latter previously oxidized. Complex immobilisation on graphite oxide via direct intercalation or via covalent attachment of an alkoxide containing the amine functions on its chain was also successfully performed. Results from several techniques have provided evidence for the effective anchoring of the amine and the alkoxide used as ligands, as well as of the metal complex. Selectivities toward the unsaturated alcohol in the hydrogenation of cinnamaldehyde comparable to that for the homogeneous complex were obtained for all the systems. The differences in activity and selectivity after recycling have been related to the ligand-support interaction type. For the graphite oxide series, the use of the alkoxide, although is leading to a less active catalysts, has advantages in terms of recyclability since both the activity and the selectivity are preserved. This is explained by the covalent attachment of the ligand through siloxane bonds, which avoids the leaching of the ligand itself or of the metal complex.

Therefore, carbon supports are promising materials for the immobilization of metal complexes, and specially GO that has been for the first time used for this purpose. In this case, the higher level of hydroxyl groups has been exploited for the covalent anchoring of an alkoxide ligand which ultimately allows the heterogenization of the metal complex.

Acknowledgment

Authors acknowledge the MICINN of Spain (Projects CTQ-2008-06839-C03-01 and -03 and EUI2008-00185 and -00205) for financial support.

References

[1] A. Choplin, F. Quignard, Coord. Chem. Rev. 178–180 (1998) 1679.
[2] P. McMorn, G.J. Hutchings, Chem. Soc. Rev. 33 (2004) 108.
[3] D.E. De Vos, M. Dams, B.F. Sels, P.A. Jacobs, Chem. Rev. 102 (2002) 3615.
[4] J.M. Fraile, J.I. García, C.I. Herrerías, J.A. Mayoral, E. Pires, Chem. Soc. Rev. 38 (2009) 695.
[5] P. Serp, J.L. Figueiredo, Carbon Materials for Catalysis, Ed Wiley, New Jersey, 2009.
[6] F. Rodriguez-Reinoso, Carbon 36 (1998) 159.
[7] A.R. Silva, M. Martins, M.M.A. Freitas, J L Figueiredo, C. Freire, B. de Castro, Eur. J. Inorg. Chem. (2004) 2027.
[8] C. Willocq, S. Hermans, M. Devillers, J. Phys. Chem. C 112 (2008) 5533–5541.

[9] S. Niyogi, E. Bekyarova, M.E. Itkis, J.L. McWilliams, M.A. Hamon, R.C. Haddon, J. Am. Chem. Soc. 128 (2006) 7720.
[10] A.B. Bourlinos, D. Gournis, D. Petridis, T. Szabó, A. Szeri, I. Dékány, Langmuir 19 (2003) 6050.
[11] S. Wang, P.-J. Chia, L.-L. Chua, L.-H. Zhao, R.-Q. Png, S. Sivaramakrishnan, M. Zhou, R. G.-S. Goh, R.H. Friend, Andrew T.-S. Wee, Peter K.-H. Ho, Adv. Mater. 20 (2008) 3440.
[12] G. Wang, X. Shen, B. Wang, J. Yao, J. Park, Carbon 47 (2009) 359.
[13] Y. Matsuo, T. Fukunaga, T. Fukutsuka, Y. Sugie, Carbon 42 (2004) 2117.
[14] Y. Matsuo, Y. Nishino, T. Fukutsuka, Y. Sugie, Carbon 45 (2007) 1384.
[15] Y. Matsuo, S. Higashika, K. Kimura, Y. Miyamoto, T. Fukutsuka, Y. Sugie, J. Mater. Chem. 12 (2002) 1592.
[16] Y. Li, W. Gao, L. Ci, C. Wang, P.M. Ajayan, Carbon 48 (2010) 1124.
[17] G. Goncalves, P.A.A.P. Marques, C.M. Granadeiro, H.I.S. Nogueira, M.K. Singh, J. Grácio, Chem. Mater. 21 (2009) 4796.
[18] M. Longhi, V. Bertacche, C.L. Bianchi, L. Fomaro, Chem. Mater. 18 (17) (2006) 4130–4136.
[19] M.-L. Sham, J.-K. Kim, Carbon 44 (2006) 768.
[20] A. Guerrero-Ruiz, P. Badenes, I. Rodríguez-Ramos, Appl. Catal. A: Gen. 173 (1998) 313.
[21] B.C. Brodie, Philos. Trans. Roy. Soc. Lond. 149 (1859) 249.
[22] A. Guerrero-Ruiz, P. Ferreira-Aparicio, M.B. Bachiller-Baeza, I. Rodriguez-Ramos, Catal. Today 46 (2–3) (1998) 99.
[23] M. Herrera-Alonso, A.A. Abdala, M.J. McAllister, I.A. Aksay, R.K. Prud'homme, Langmuir 23 (2007) 10644.
[24] A.-Y. Park, H. Kwon, A.J. Woo, S.-J. Kim, Adv. Mater. 17 (2005) 106.
[25] F. Barroso-Bujans, S. Cerveny, A. Alegría, J. Colmenero, Carbon 48 (2010) 3277.
[26] A. Lerf, H. He, M. Forster, J. Klinowski, J. Phys. Chem. B 102 (1998) 4477.
[27] C.-H. Chiang, N.-I. Liu, J.L. Koenig, J. Colloid Interf. Sci. 86 (1982) 26.
[28] M.-C.B. Salon, M. Abdelmouleh, S. Boufi, M.N. Belgacem, A. Gandini, J. Colloid. Interf. Sci. 289 (2005) 249.
[29] A.K. Chauhan, D.K. Aswal, S.P. Koiry, S.K. Gupta, J.V. Yakhmi, C. Sürgers, D. Guerin, S. Lenfant, D. Vuillaume, Appl. Phys. A 90 (2008) 581.
[30] F. Barroso-Bujans, S. Cerveny, R. Verdejo, J.J. del Val, J.M. Alberdy, A. Alegría, J. Colmenero, Carbon 48 (2010) 1079.
[31] Y. El-Sayed, T.J. Bandosz, Langmuir 21 (2005) 1282.
[32] R. Sokoll, H. Hobert, I. Shmuck, J. Catal. 121 (1990) 153.
[33] H.F. Gorgulho, J.P. Mesquita, F. Gonçalves, MFR. Pereira, J.L. Figueiredo, Carbon 46 (2008) 1544.
[34] T. Kijima, S. Watanabe, M. Machida, Inorg. Chem. 33 (1994) 2586.
[35] Y. Matsuo, T. Miyabe, T. Fukutsuka, Y. Sugie, Carbon 45 (2007) 1005.
[36] O. Krenawahjuesa, R.J. Gorte, D. de Oliveira, L.Y. Lau, Catal. Lett. 82 (2002) 155.
[37] M. Mermoux, Y. Chabre, A. Rousseau, Carbon 29 (3) (1991) 469.
[38] T. Szabó, O. Berkesi, P. Forgó, K. Josepovits, Y. Sanakis, D. Petridis, I. Dékény, Chem. Mater. 18 (2006) 2740.
[39] S. Stankovich, R.D. Piner, SonBinh T. Nguyen, R.S. Ruoff, Carbon 44 (2006) 3342.
[40] Á. Zsigmond, I. Balatoni, K. Bogár, F. Notheisz, F. Joó, J. Catal. 227 (2004) 428.
[41] A. Ghosh, R. Kumar, Microporous Mesoporous Mater. 87 (2005) 33.
[42] J.W. Robinson (Ed.), Practical Handbook of Spectroscopy, CRC Press, Florida, 1991, pp. 183–418.
[43] E. Asedegbega-Nieto, B. Bachiller-Baeza, A. Guerrero-Ruíz, I. Rodríguez-Ramos, Appl. Catal. A: Gen. 300 (2006) 120.
[44] P.G. Jessop, Y. Hsiao, T. Ikariya, R. Noyori, J. Am. Chem. Soc. 118 (1996) 344.
[45] R. Noyori, T. Ohkuma, Angew. Chem. Int. Ed. 40 (2001) 40.